THE ASTROPHYSICAL JOURNAL, 515:275–285, 1999 April 10

THE MAGNETIC FIELD OF THE NGC 2024 MOLECULAR CLOUD

R. M. CRUTCHER AND D. A. ROBERTS
Astronomy Department, University of Illinois, Urbana, IL 61801
T. H. TROLAND
Physics and Astronomy Department, University of Kentucky, Lexington, KY 40506
AND
W. M. GOSS
National Radio Astronomy Observatory, Socorro, NM 87801
Received 1998 September 18; accepted 1998 November 13

ABSTRACT

We have carried out Very Large Array (VLA)[1] Zeeman observations of absorption lines of H I and OH toward the molecular cloud associated with the NGC 2024 (Orion B) H II region. The synthesized beam diameters are $68'' \times 52''$, p.a. $= 38°$, and $81'' \times 65''$, p.a. $= -6°$, for OH and H I, respectively. The absorption lines could be mapped over the NGC 2024 continuum source, which has an extent (at the 1 Jy beam^{-1} level) of $\Delta\alpha \approx 7'$ by $\Delta\delta \approx 5'$. The maps of the magnetic field, together with comparisons with additional data from the published literature, lead to the following conclusions: (1) The magnetic field comes from a line subcomponent at $v_{\rm LSR} \approx 10.2$ km s^{-1}, which corresponds in velocity and in spatial morphology with the northern dense molecular ridge in NGC 2024. (2) $B_{\rm los}$ varies from 0 to the northeast of the northern molecular ridge to almost 100 μG to the southwest. The variation in $B_{\rm los}$ may be due to the field being mainly in the plane of the sky to the northeast but having a significant line-of-sight component to the southwest. (3) Velocities in the cloud are supersonic but approximately equal to the Alfvén velocity, which is consistent with motions being dominated by magnetohydrodynamical waves rather than thermal motion or hydrodynamical turbulence. (4) The mass-to-magnetic flux ratio is supercritical, which suggests that the static magnetic field does not support the cloud against collapse. Simple virial estimates of the relative importance of gravitational, kinetic, and magnetic energies show that the ratio of kinetic/gravitational energy is about 0.5, while the magnetic/gravitational energy ratio is less than 0.1. At face value, these results imply that the cloud is supported mainly by nonthermal motions rather than by the static magnetic field. However, since we only measure directly the line-of-sight component of $\boldsymbol{B}$, this result is not conclusive.

Subject headings: ISM: clouds — ISM: individual (NGC 2024) — ISM: kinematics and dynamics — ISM: magnetic fields — ISM: molecules

1. INTRODUCTION

The evolution of interstellar clouds as they form new stars is one of the fundamental topics of astrophysics. Theoretical studies suggest that magnetic fields may play an important or even crucial role in the star formation process. Although observations of densities, temperatures, kinematics, and structures in dense interstellar clouds have yielded a considerable volume of information about these crucial physical parameters, our information about magnetic fields is much more sparse. As part of a long-term project to observe magnetic fields in dense interstellar clouds, we have carried out circular polarization mapping observations with the VLA of the H I and the two main OH absorption lines toward the H II region NGC 2024 (Orion B); we use the Zeeman effect to derive line-of-sight magnetic fields.

The NGC 2024 region has been the object of many observational studies, because it is an excellent laboratory for the study of various stages of star formation. The region has visible B stars, an embedded infrared cluster, dense molecular gas, molecular outflows, and possibly isothermal protostars. Crutcher et al. (1986) discussed a model of the region based on published observations and on their VLA H_2CO absorption-line maps. The molecular cloud has an elongated (north-south) morphology similar to that of the dust lane seen projected onto the optical H II region. Molecular gas in this dust lane is seen in absorption against the continuum of the H II region with a velocity of peak absorption $v_{\rm LSR} \approx 9.3$ km s^{-1}. However, millimeter-wave molecular lines (such as high-J transitions of CS) that sample high gas densities (e.g., Snell et al. 1984) have a typical velocity $v_{\rm LSR} \sim 10$–12 km s^{-1}. This led to the suggestion that the H II region is embedded in the near side of the cloud with the bulk of the dense molecular gas behind it. The expanding ionized gas has broken out of the molecular cloud to the east and west, and, in addition, is expanding northward away from a sharply defined ionization front to the south. Barnes et al. 1989 provided a more detailed discussion of the morphology of the region and presented numerous figures that show the relationships between the various constituents. Van der Werf et al. (1993) mapped H I absorption toward NGC 2024 with the VLA. These maps show three kinematically distinct layers, at $v_{\rm LSR} \approx 6.6$, 9.6, and 12 km s^{-1}, which they interpreted, respectively, as a shocked photodissociation region (PDR) at the H II velocity, a dense unshocked PDR, and a cloud halo. The OH and H_2CO maps show only the latter two velocity components, with

[1] The VLA is operated by the National Radio Astronomy Observatory (NRAO). The NRAO is a facility of the National Science Foundation operated under cooperative agreement by Associated Universities, Inc.

the main molecular absorption occurring in the unshocked PDR component.

Mezger et al. (1988) mapped dust emission toward NGC 2024 at 1300 and 350 μm and reported the detection of six dense ($n_{\rm H} \sim 10^8$–10^9 cm^{-3}), cold ($T_d \approx 16$ K) isothermal protostars (labeled FIR 1–6). Since these clumps were not seen in molecular tracers of high-density regions, they suggested that molecules were heavily depleted from the gas by accretion onto dust grains. This paper triggered numerous additional studies (Moore et al. 1989; Schulz et al. 1991; Chandler, Moore, & Emerson 1992; Mezger et al. 1992; Mauersberger et al. 1992; Wilson, Mehringer, & Dickel 1995; Chandler & Carlstrom 1996; Wiesemeyer et al. 1997) of the dense, cold material toward NGC 2024. The result of these studies appears to be that maps of high-density molecular tracers (such as the $J = 7 \rightarrow 6$ line of CS) show that there is a ridge of warm, dense molecular gas in which the dust clumps are embedded. However, there is not a detailed positional correspondence between the dust and the gas clumps. Mezger et al. (1992) provided the following summary of the NGC 2024 molecular cloud core: There is a 0.3×0.5 pc envelope with $M_{\rm H}({\rm total}) \approx 300\ M_\odot$ and $\langle n_{\rm H} \rangle \approx 1 \times 10^5$ cm^{-3}. A 0.04×0.3 pc, roughly north-south ridge is at the center of the envelope, with $M_{\rm H}({\rm total}) \approx 140\ M_\odot$ and $\langle n_{\rm H} \rangle \approx 5 \times 10^6$ cm^{-3}. Embedded close to the center of the ridge are seven cold clumps (FIR 1–7) seen only in dust emission with $\langle M_{\rm H} \rangle \approx 10\ M_\odot$, $\langle n_{\rm H} \rangle \approx 2 \times 10^8$ cm^{-3}.

Observations of magnetic field strengths and morphology in the region of active and ongoing star formation are essential in order to complete the measurements of important physical parameters. Hildebrand et al. (1995) have mapped far-infrared (FIR) linearly polarized emission from dust toward NGC 2024. The linear polarization directions are perpendicular to the direction of the magnetic field in the plane of the sky. These observations show that the magnetic field is oriented in generally an east-west direction, perpendicular to the long axis of the ridge of dense molecular gas described by Mezger et al. (1992). In addition, there is some small-scale structure in the immediate vicinity of the ridge. No information about the magnitude of the magnetic field is directly available from these data. Crutcher & Kazès (1983) reported the detection of the Zeeman effect in the OH 1665 and 1667 MHz absorption lines toward NGC 2024 and found $B_{\rm los} = +38 \pm 1$ μG. Because this measurement was made with the single-dish Nançay radio telescope, the result refers to a global average of $B_{\rm los}$, weighted by the strength of the OH absorption lines. Van der Werf et al. (1993) attempted to map the magnetic field with VLA synthesis observations of the H I line, but limited sensitivity required them to spatially average in order to obtain a marginal detection of Stokes parameter V.

In order to map the strength of the magnetic field toward NGC 2024, we have carried out very sensitive Zeeman observations of H I and OH absorption lines and report the results in this paper.

2. OBSERVATIONS

Observations were carried out with the VLA D array on 1996 July 19 and 24 (OH) and 1991 April 6 and 8 (H I). The two OH main lines were observed simultaneously; opposite senses of circular polarization were observed simultaneously for both OH and H I, with a front-end transfer switch being used to reverse the polarizations every 10 minutes in order to reduce possible instrumental effects. Further information about our observations is given in Table 1.

The observational and data processing procedures were similar to those we have used in previous VLA Zeeman mapping projects (Roberts et al. 1993; Roberts, Crutcher, & Troland 1995). We took care during the editing process to flag both the right and left circular polarization data (RCP and LCP, respectively) whenever any visibility record was to be deleted, so the UV coverage and hence the dirty synthesized beams were identical for the two polarizations. Calibration of the absolute flux density, complex gains, and the bandpass response was carried out with the AIPS package of the NRAO. Data from the line-free channels near the edges of the band were combined to produce a continuum visibility database. The continuum was subtracted from the line data in the visibility plane with the AIPS program UVLIN. Final imaging, map processing, visualization, and Zeeman analysis were carried out with the MIRIAD system of the Berkeley-Illinois-Maryland Association (BIMA). Imaging used natural weighting and a cell size of 15″. Channel maps were made separately for RCP and LCP. Because we found that noise in the bandpass data could dominate noise in the source data for Stokes parameter V maps, we produced Stokes V maps using non–bandpass-corrected visibility data; the Stokes I

TABLE 1

OBSERVATIONAL PARAMETERS

Item	OH Lines	H I Line
Frequency (MHz)	1665, 1667	1420
Observing dates	1996 Jul 19, 24	1991 Apr 6, 8
Total observing time (hr)	21	16
Primary beam HPBW (arcmin)	25	30
Synthesized beam	68″ × 52″, p.a. = 38°	81″ × 65″, p.a. = −6°
Phase and pointing centers	$\alpha_{1950} = 5^{\rm h}39^{\rm m}12^{\rm s}$, $\delta_{1950} = -1°56'00''$	$\alpha_{1950} = 05^{\rm h}38^{\rm m}31^{\rm s}$, $\delta_{1950} = -1°55'20''$
Total bandwidth (kHz)	195.3125 (35 km s^{-1})	195.3125 (41 km s^{-1})
Center velocity (km s^{-1})	+10	+9
Channel separation (kHz)	1.526 (0.275 km s^{-1})	1.526 (0.322 km s^{-1})
Spectral smoothing	None	On-line Hanning
Flux calibrator	3C48, 3C286	3C48
Phase calibrator	0500+019	0605−08
Line channel rms noise (mJy beam^{-1})	6.9	7.7
Correlator mode	4IF	2IF

maps were bandpass-corrected. The strong absorption features in the continuum-subtracted I cube created significant sidelobe effects, which, in addition to systematic velocity gradients, caused confusion among the various features. The CLEAN algorithm was used to deconvolve each of the spectral channels in the Stokes I cube to residual level of 40 and 10 mJy beam^{-1} for H I and OH, respectively. For the Stokes V data the sidelobe effects were below the rms noise level and were not significant, so no deconvolution was carried out. Zeeman analysis was carried out with the MIRIAD routine ZEEMAP. The unCLEANED Stokes I and V data were used to correct V for polarization leakage caused by antenna gain errors (Roberts et al. 1993).

We also used the NRAO 12 m telescope to carry out an on-the-fly mapping of the NGC 2024 region in the $J = 1 \rightarrow 0$ line of $C^{18}O$. The velocity resolution was 0.27 km s^{-1}, and the FWHP beam was 58″, which are very similar to the velocity resolutions and synthesized beams of our VLA observations. At the 415 pc distance of NGC 2024 (Anthony-Twarog 1982), $1' = 0.12$ pc.

3. ANALYSIS

The H I and OH Stokes I absorption toward NGC 2024 have already been extensively discussed by van der Werf et al. (1993) and Barnes et al. (1989), respectively. The new H I data have about half the noise level of the earlier maps because of improved L-band receivers on the VLA. This is not sufficient to allow us to improve on the earlier discussion of the H I absorption, but it is crucial in allowing us to map the magnetic field. The earlier OH maps (Barnes et al. 1989) included both D and B array data, although smoothing to a beam size of 13″ was necessary in order to study the OH absorption. They were not polarization observations and therefore contained no information about the OH Zeeman effect. Our new OH maps are significantly more sensitive than the Barnes et al. (1989) ones, because of improved receivers but especially because of our larger synthesized beam size. This improved sensitivity gives new information about the distribution of OH absorption, which is discussed below.

Figure 1 shows the Stokes I and V spectra for the OH 1665 and 1667 MHz lines at the position of maximum $B_{\rm los}$. It is clear that while the Stokes V signal comes from within the main velocity component, it does not come from the entire component. That is, dI/dv is not an intensity-scaled replica of the Stokes V spectra. The positive maximum in Stokes V occurs at $v_{\rm LSR} \approx 9.6$ km s^{-1}, which is roughly the velocity of peak absorption in the Stokes I spectra. The center of the Stokes V spectra, where $V = 0$, occurs at $v_{\rm LSR} \approx 10.2$ km s^{-1}. This is the same situation found by Crutcher & Kazès (1983) with their single-dish data; they found that the Stokes parameter V spectrum that they observed did not come from the entire line profile but from a subcomponent with $v_{\rm LSR} \approx 10.2$ km s^{-1} and $\Delta v \approx 1.0$ km s^{-1}. (The velocity of the component responsible for a Zeeman V spectrum is equal to the velocity of the Stokes $V = 0$ point, whereas the line width may be inferred from the velocity displacement of the positive and negative peaks in the V spectrum.) We attempted to deconvolve the multiple velocity component structure of the OH line blend by Gaussian fitting but were unable to obtain reliable results, probably because of the insufficient velocity resolution of the VLA data. At all positions the Stokes V spectra imply $v_{\rm LSR} = 10.2 \pm 0.2$ km s^{-1} and $\Delta v = 1.1 \pm 0.2$ km s^{-1}. However, the amplitude of this component could not be determined. Hence, in order to derive the magnetic field from our VLA data, we followed Crutcher & Kazès (1983) and assumed that the Stokes V signal was produced by a velocity subcomponent with $v_{\rm LSR} \approx 10.2$ km s^{-1}, $\Delta v \approx 1.1$ km s^{-1}, and intensity equal to the observed intensity at $v_{\rm LSR} \approx 10.2$ km s^{-1}. It is likely that there is some contribution to the OH absorption intensity at $v_{\rm LSR} = 10.2$ km s^{-1} from the wings of other line components, so the actual intensity of the $v_{\rm LSR} = 10.2$ km s^{-1} component is less than we have assumed. This overestimate of the intensity of the component responsible for the Stokes V signal would result in an *underestimate* of the actual $B_{\rm los}$.

Zeeman observations are subject to two possible spurious effects: (1) For the OH lines, weak circularly polarized masers may be present and produce Stokes V signals. (2) The most important instrumental effect can occur if the two circularly polarized beams point in different directions (beam squint); a velocity gradient across a source could then produce a Stokes V signal apparently identical to the Zeeman effect. Beam squint is of special concern for single-dish observations, but for aperture-synthesis observations with identical UV-plane coverage in the two circular polarizations, the synthesized beams are identical, and there is no beam squint. The OH Zeeman results reported here provide direct and convincing evidence that the observed Stokes V signals are due to the Zeeman effect and that our maps of $B_{\rm los}$ are valid. Instrumental effects would produce Stokes V signals proportional in strength to the Stokes I signals. Figure 1 shows that this is clearly not the case: the Stokes V signal for the 1667 MHz line is considerably weaker than that for the 1665 MHz line. The Zeeman splitting factors for the two OH lines are not the same but have a ratio $Z_{1665}/Z_{1667} = 1.67$, which leads to the stronger Stokes V signal for the 1665 MHz line in Figure 1. We computed $B_{\rm los}$ separately for the two OH lines and found that the results were the same within the noise. If the Stokes V signals were due to weak, circularly polarized masers, one would not expect the signals to be spatially extended or to yield the same magnetic field strength from the two OH lines. The agreement we find in the inferred field strength over a spatially extended area eliminates the possibility that the observed polarization is due to a weak polarized maser and not to the Zeeman effect. The agreement of $B_{\rm los}$ found separately from two lines with different Zeeman splitting factors also shows that the Stokes parameter V signals that we observe are in fact due to the Zeeman effect rather than to possible instrumental effects.

For the H I line toward NGC 2024, the blending of three major velocity components (van der Werf et al. 1993) complicated the Zeeman analysis. This is similar to the situation for Cas A (Schwarz et al. 1986) and for W3 (Roberts et al. 1993), where there were two blended, optically thick velocity components. This resulted in suppression of that half of the Zeeman V pattern for each velocity component that would occur at velocities where the other component was optically thick. For NGC 2024, a Stokes V signal is seen with high signal-to-noise ratio only at the most positive velocity side of the blended, optically thick line profiles (Fig. 2). We interpret this as a line-of-sight magnetic field in one velocity component, with the corresponding Stokes V signal from the other side of the line being suppressed by the optical depth of a lower velocity component. We therefore carried out the Zeeman analysis of the H I data by limiting

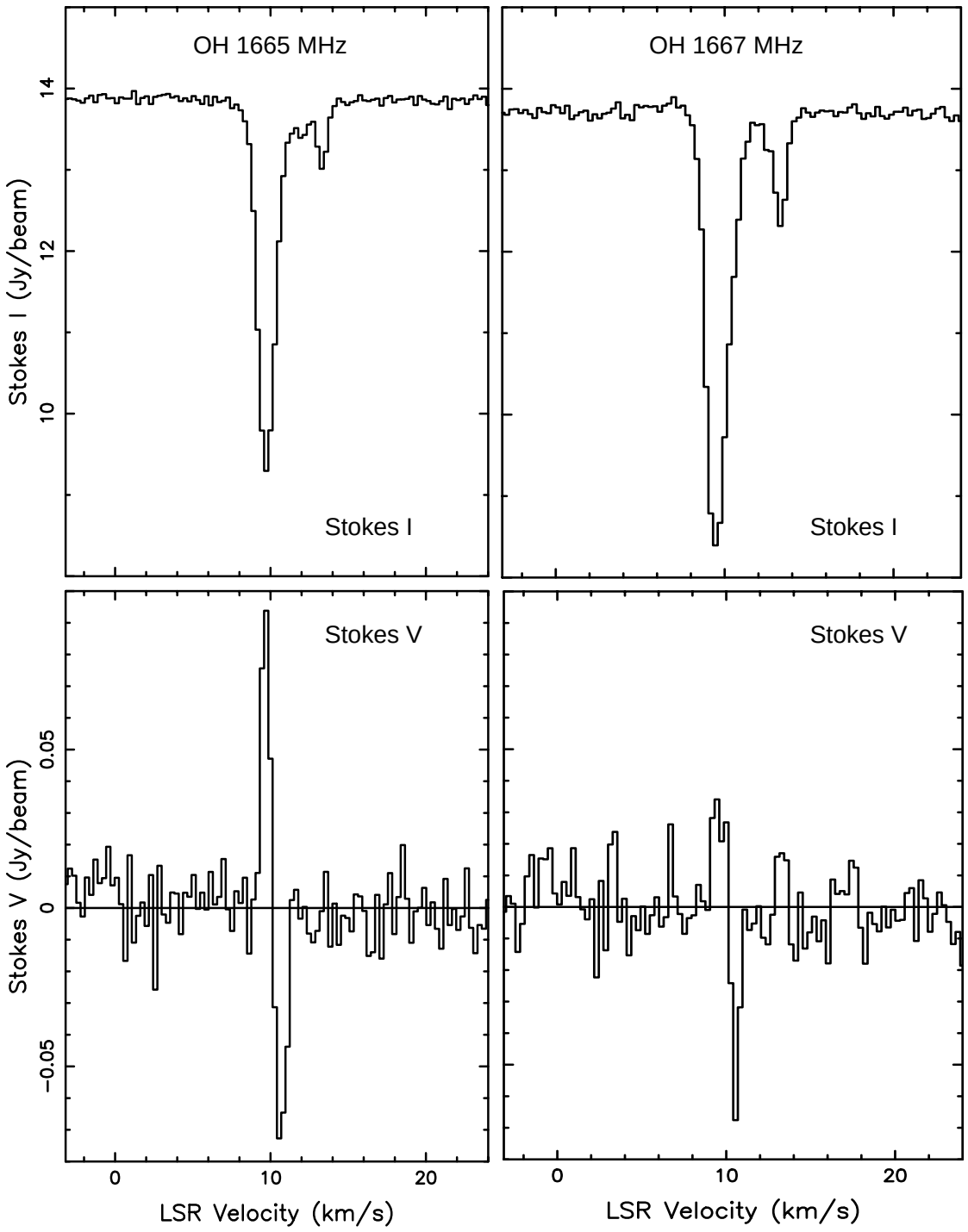

FIG. 1.—OH Stokes I and V 1665 (*left*) and 1667 MHz (*right*) spectra at the position of the peak in B_{los}. This peak B_{los} position is $\alpha(1950) = 05^h39^m09^s$, $\delta(1950) = -01°56'30''$.

the velocity range to the positive velocity side of the line, $v_{LSR} = 9.6$–18.4 km s^{-1}. Our experience suggests that this procedure will recover B_{los} successfully in spite of having only half of the Zeeman V spectrum available.

4. RESULTS

Figure 3 shows as a color image the line-of-sight magnetic field derived from our VLA observations of OH 1665 and 1667 MHz absorption. We have averaged the results obtained separately for the two lines to produce this image: B_{los} is shown wherever the signal-to-noise ratio $B_{los}/\sigma_B \geq 3$ or $\sigma_B < 12$ μG. The latter constraint was used to make it possible to map the field in regions with near-zero B_{los} where σ_B was low. The peak value of $B_{los} \approx +87 \pm 5.5$ μG occurs near the southwest edge of the region mapped; the line profiles shown in Figure 1 are those at this position.

Figure 3 also shows as a contour map the line-of-sight magnetic field (B_{los}) map derived from our VLA observations of H I absorption; B_{los} is shown wherever the signal-to-noise ratio $B_{los}/\sigma_B \geq 3$ or $\sigma_B < 8$ μG. The H I profiles

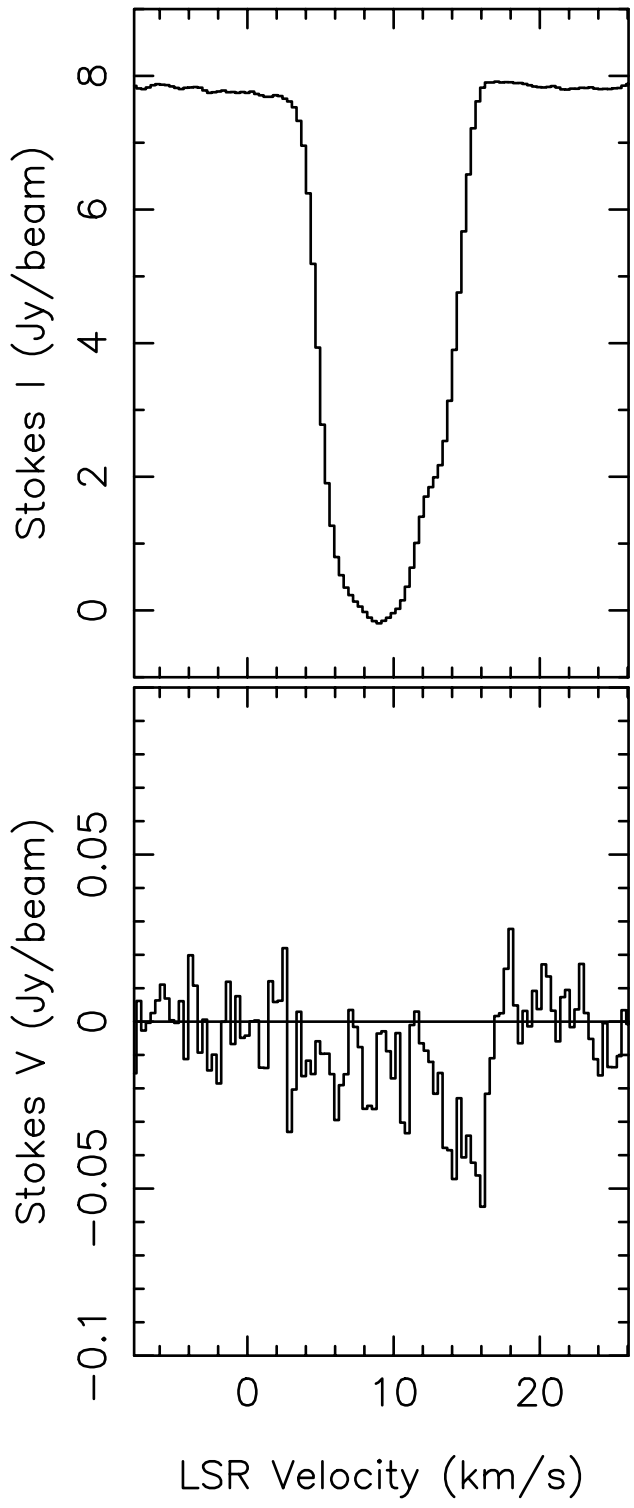

FIG. 2.—H I Stokes I and V spectra at the position of the OH spectra in Fig. 1.

shown in Figure 2 are from the same position as the OH profiles shown in Figure 1: $B_{\rm los}$ shows a maximum $B_{\rm los} \approx +52 \pm 9$ μG near the southwest corner of the region mapped. The agreement between the morphologies of the magnetic field maps obtained from OH and H I is striking. The difference between $B_{\rm los} \approx +52 \pm 9$ μG derived from H I and $B_{\rm los} \approx +87 \pm 5.5$ μG derived from OH appears to be significant, especially since the OH result is effectively a lower limit because of the likely overestimate of the intensity of the OH component producing the Zeeman effect.

The velocity of the component producing the H I Stokes V signal is far from clear. The H I profiles clearly show the blended velocity structure that was discussed by van der Werf et al. (1993). The maximum Stokes V signal occurs between 13.4 km s$^{-1} \lesssim v_{\rm LSR} \lesssim$ 16.6 km s^{-1} and appears to be due to a magnetic field in the $v_{\rm LSR} \approx 13$ km s^{-1} component. However, there is no Stokes V signal in the OH velocity component at this velocity (Fig. 1). The striking agreement between the morphologies of the magnetic fields mapped in OH and H I (Fig. 3) suggests that the field arises in the same velocity component, at $v_{\rm LSR} \approx 10.2$ km s^{-1}. Blending of the optically thick H I components makes it impossible to be certain of this, but we believe it most likely that the H I field arises in the $v_{\rm LSR} \approx 10.2$ km s^{-1} component and not in the $v_{\rm LSR} \approx 13$ km s^{-1} component. Further discussion of $B_{\rm los}$ toward NGC 2024 will be based on the OH results.

The H I data also show an apparently significant Stokes V signal (at about the 4 σ level) to the east of the region shown in Figure 3. There is no corresponding field in OH; this is not significant, however, because there is essentially no OH absorption in this region. We do not believe that the significance of this possible field in H I to the east is sufficiently high to claim it as real at this time; it will not be further discussed here.

5. DISCUSSION

It is of crucial importance to understand what region of the NGC 2024 molecular cloud is sampled by the Zeeman observations. The velocity of the component in which the Zeeman effect is observed (based on the Stokes V spectra) is $v_{\rm LSR} \approx 10.2$ km s^{-1}. In addition to the V spectra, there is other evidence that there is a distinct OH component at this velocity. Figure 4 shows the cores of the 1665 and 1667 MHz lines at the position of maximum magnetic field strength. The velocity of maximum absorption of the 1667 MHz line is $v_{\rm LSR} \approx 9.3$ km s^{-1}, whereas that of the 1665 MHz line is $v_{\rm LSR} \approx 9.7$ km s^{-1}. This shift can be accounted for if there is a very optically thick subcomponent at $v_{\rm LSR} \approx 10.2$ km s^{-1}. Figure 4 also shows the ratio of the two OH lines over the core velocities. The optically thin LTE line ratio is 1.8, while for a very large optical depth the ratio would be 1; $I_{1667}/I_{1665} \approx 1$ for the LSR velocity range 9.7–10.5 km s^{-1}. It appears that the line optical depth is very large at $v_{\rm LSR} \approx 10.1$ km s^{-1} and is much smaller at $v_{\rm LSR} \lesssim 9.5$ km s^{-1}. Hence, it appears from the Stokes I spectra alone that there is a distinct velocity component within the OH lines with velocity and line width that agree with those parameters derived from the Stokes V spectra.

The greater sensitivity of our OH absorption-line maps (albeit at lower angular resolution) in comparison with the earlier study (Barnes et al. 1989) makes it possible to investigate the nature of the $v_{\rm LSR} = 10.2$ km s^{-1} OH component. Figures 5 and 6 show channel color images of the line optical depth of the 1665 MHz OH line at $v_{\rm LSR} = 9.7$ and 10.2 km s^{-1}. Superposed on the color images are the contour channel maps of the $C^{18}O$ emission from our NRAO 12 m observations at the same respective velocities. The positions of the FIR very dense dust clumps and the position of peak $B_{\rm los}$ are also marked.

At the velocity of maximum 1665 MHz OH line absorption ($v_{\rm LSR} = 9.7$ km s^{-1}), there is a general correspondence

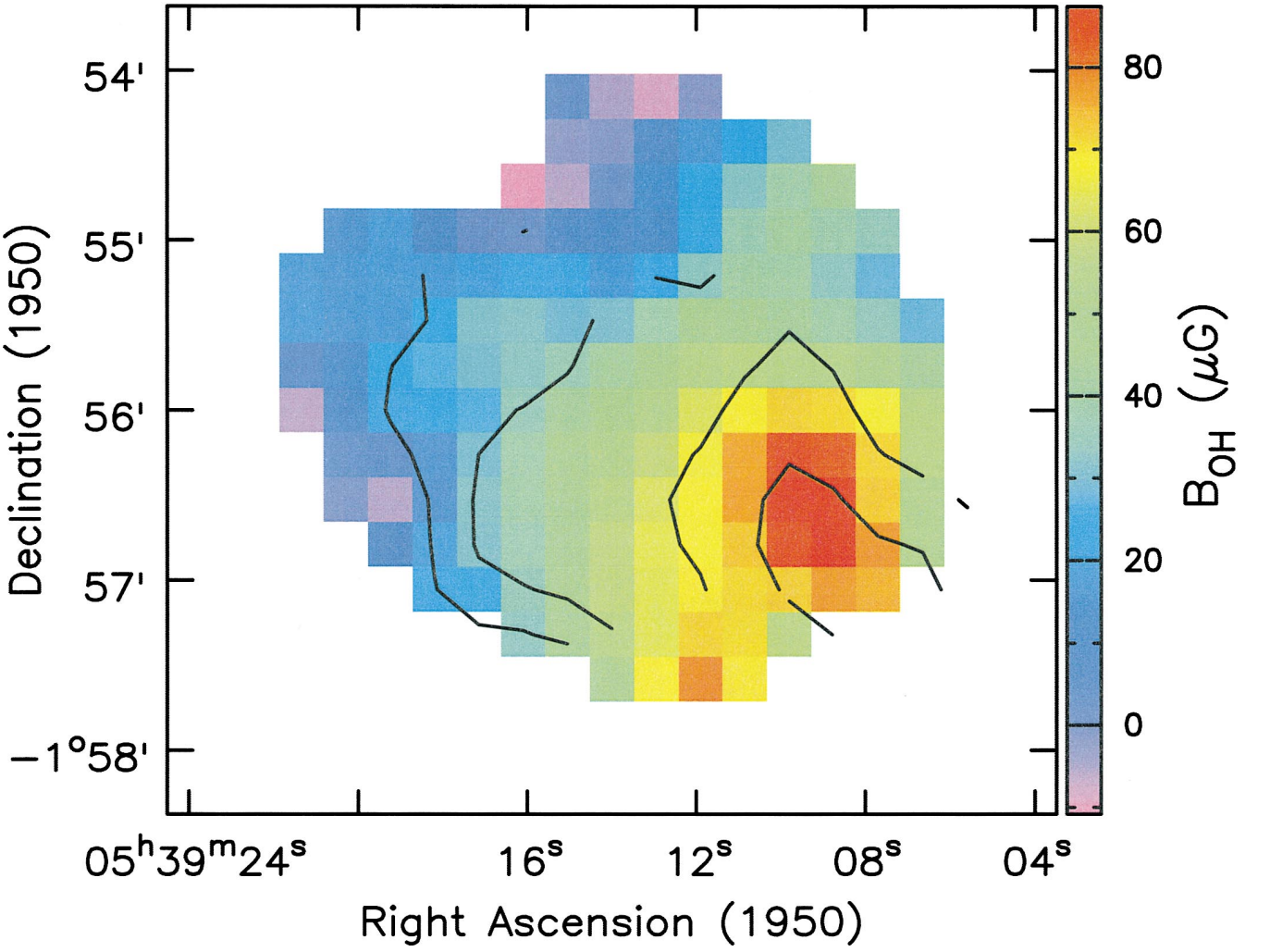

FIG. 3.—Maps of B_{los} from OH (*color image*) and H I (*contours*). Contour levels are 15, 30, and 45 μG.

between the spatial distributions of OH absorption, $C^{18}O$ emission, and the FIR dust clumps. However, the $C^{18}O$ is displaced slightly to the east of the very dense ridge line defined by the FIR dust clumps, and the OH absorption is displaced still farther to the east. Schulz et al. (1991) pointed out that the eastern boundary of the northern molecular ridge (in which the FIR dust clumps are embedded) is sharper than the western boundary and that the easternmost tip of the arc formed by the FIR sources closely borders the northern peak of the radio H II region. They suggested that the dense northern molecular ridge may represent the dense, cooled, postshock layer preceding the ionization front. Hence, the spatial displacements may be due to the interaction front seen edge-on between the ionized and molecular gas. OH is generally not very abundant at high gas densities, but it may have a large abundance in a photodissociation region (PDR) because of photodissociation of H_2O. We suggest that the large eastward displacement of the peak OH absorption may be due to an enhanced abundance of OH in the PDR.

At $v_{LSR} = 10.2$ km s^{-1} the situation is rather different. The $C^{18}O$ and FIR sources now coincide (considering the $\sim 1'$ resolution of the $C^{18}O$ map). The OH absorption has a relative minimum near the position of maximum OH optical depth at $v_{LSR} = 9.7$ km s^{-1}, with a region of slightly enhanced line absorption west of this minimum that corresponds spatially with the $C^{18}O$ and FIR sources. The velocity of this OH component is more positive than the material that Crutcher et al. (1986) and Barnes et al. (1989) argue is relatively low-density molecular gas in front of the H II region and associated with the dark dust lane seen projected onto it. In fact, $v_{LSR} = 10.2$ km s^{-1} is similar to the velocities of the dense gas in the northern molecular ridge associated with the very dense dust clumps, FIR 1–4. The BIMA synthesis maps of $C^{18}O$ (Wilson et al. 1995) gave the following line parameters for FIR 1–4, respectively: $(v_{LSR}, \Delta v) = (10.3, 0.7), (9.5, 0.7), (10.6, 0.9)$, and $(10.8, 1.0)$, or $\langle v_{LSR} \rangle \approx 10.3$ km s^{-1}. Similarly, for the high-density tracer ^{34}CS ($J = 5 \rightarrow 4$), Schulz et al. (1991) gave the following: $(v_{LSR}, \Delta v) = (10.4, 1.1), (10.2, 1.4), (10.6, 1.6), (11.0, 1.4)$, or $\langle v_{LSR} \rangle \approx 10.5$ km s^{-1}. It appears that the OH feature that corresponds spatially and kinematically (considering the poor angular resolution of the OH data) with the dense northern molecular ridge is very optically thick OH directly associated with the ridge.

Previously it had been concluded (Crutcher et al. 1986; Barnes et al. 1989) that all of the dense gas at $v_{LSR} > 10$ km s^{-1} is behind the H II region. One possibility is that *all* of the molecular gas is in front of the H II region (and in the dark lane seen optically). The lack of (very much) OH and H_2CO absorption at $v_{LSR} \gtrsim 10$ km s^{-1} would then have to be a result of much lower than typical abundances of these

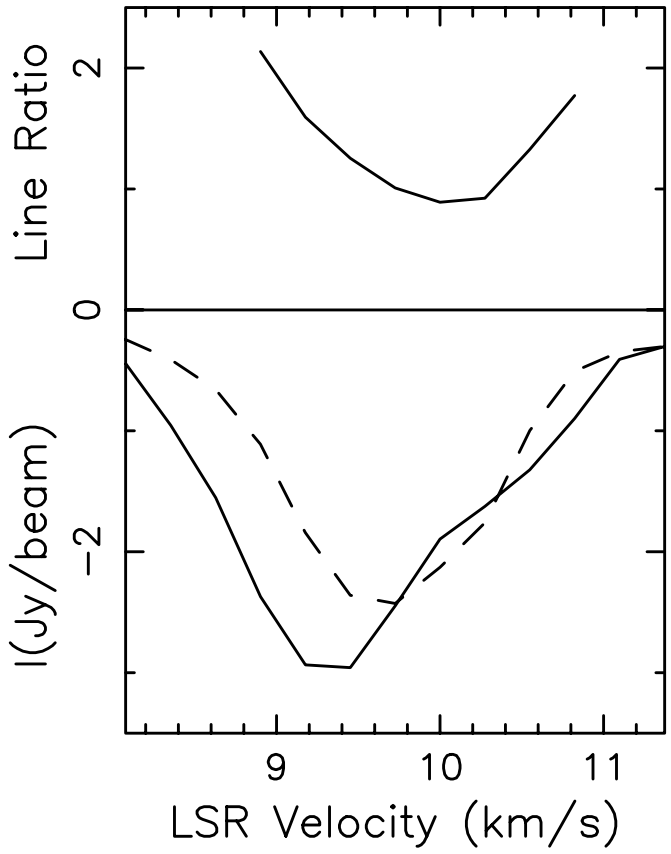

FIG. 4.—*Bottom*: Plots of the core velocity range of the 1667 (*solid line*) and 1665 (*dashed line*) MHz OH lines at the position of maximum B_{los}. *Top*: Ratio of the two OH lines.

molecules because of photodissociation and large depletions from the gas phase. However, the OH line ratio suggests that the OH line optical depths in the molecular ridge region are large, not small. This picture would also be difficult to reconcile with the detailed model discussed by Barnes et al. (1989), which nicely explains the kinematical and morphological data for NGC 2024. Another possibility is that the region is very clumpy, with most of the H II region in a cavity between the lower density gas with $v_{LSR} \approx 9.5$ km s^{-1} and the higher density molecular ridge with $v_{LSR} \approx 10$–11 km s^{-1} but with some ionized gas behind the higher velocity molecular gas. Having a very small contribution to the continuum radiation from behind the molecular ridge gas could explain why the OH line optical depths could be large even though the line intensities are small. The clumpy picture seems more likely to be the correct one.

Figure 7 shows our contour map of $C^{18}O$ $J = 1 \rightarrow 0$ emission and our image of B_{los}(OH). Superposed are lines showing the linear polarization of warm dust emission at 100 μm (Hildebrand et al. 1995); the direction of the magnetic field in the plane of the sky is perpendicular to these polarization vectors.

The relationship between the magnetic field in the plane of the sky as inferred from measurements of linearly polarized dust emission and the magnetic field along the line of sight inferred from the Zeeman effect in absorption lines is, of course, not clear. Because the dust is likely to be hotter near the H II region, the dust emission is probably dominated by material in or near the PDR, which is likely the location of the OH and H I in the molecular envelope. Hence, the two types of measurements of the magnetic field may be more closely related than one might at first suppose. The magnetic field in the plane of the sky (which is perpendicular to the polarization vectors shown) is generally perpendicular to the elongated north-south distribution of the molecular cloud, which suggests that the dense material has collapsed along the field lines but has at least partially been prevented from collapsing across field lines by magnetic pressure. In the region of the molecular ridge there is clearly some small-scale structure in the field, with a possible inward pinch of the field lines at the position of the northern $C^{18}O$ clump. This pinch is suggestive of the hourglass morphology expected for the collapse of a molecular cloud with a strong frozen-in magnetic field.

The magnitude of B_{los} changes from 0 to the northeast of the molecular ridge to nearly 100 μG in the southwest. Although this could be a real change in the magnitude of the total field strength, it seems more likely that it is an orientation effect. Support for this suggestion comes from the fact that the amplitude of the linear dust polarization has a relative minimum at the position of maximum B_{los}. This decrease in the percentage polarization could be due to the magnetic field being in the plane of the sky to the northeast of the northern $C^{18}O$ clump and having a significant component along the line of sight to the southwest. A similar situation was found in comparing Zeeman and dust polarization maps toward M17 (Brogan et al. 1999). However, there is no direct relationship between the percentage polarization of dust emission and the magnitude of

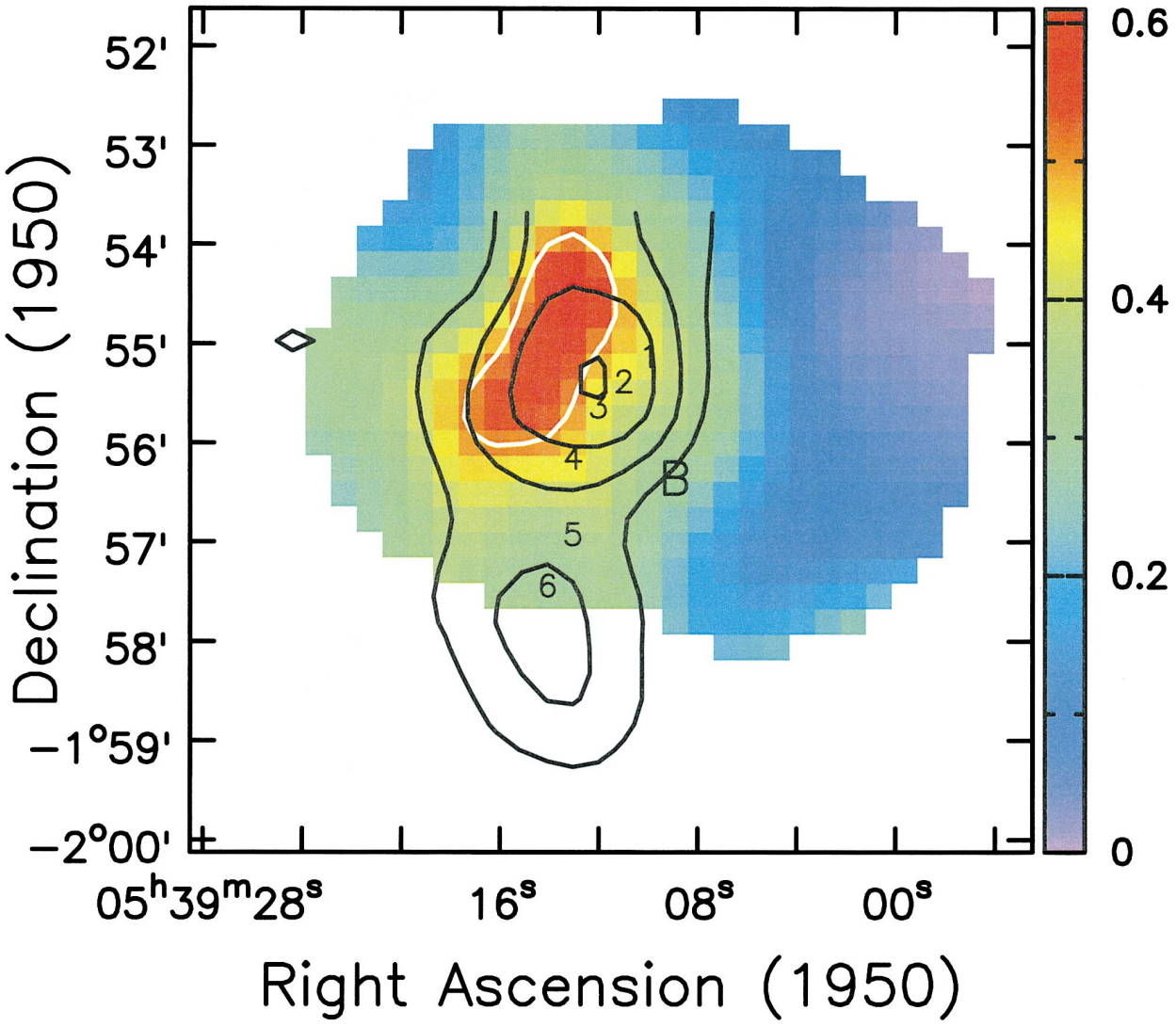

FIG. 5.—Channel maps at $v_{LSR} = 9.7$ km s^{-1} of the OH 1665 MHz line optical depth (*color image*) and the C^{18}O emission (*black contours*). Contour levels are at $T_A^* = 2, 3, 4, 5$ K. The τ(OH) = 0.5 contour is also shown in white. The positions of the dense dust clumps FIR 1–6 are indicated by the positions of the respective numbers. Finally, *B* indicates the position of maximum B_{los}.

the magnetic field in the plane of the sky; the change in percentage polarization could be due entirely to a change in dust grain properties. In any case, whether the maximum magnitude of B_{los} found to the southwest is the total magnitude of the field or whether the field is still mainly in the plane of the sky at this position cannot be determined from these data.

We can use our measurements of the magnetic field together with published determinations of other physical parameters to estimate the importance of the magnetic field in the NGC 2024 molecular cloud. Table 2 gives the relevant data. We assume that the OH Zeeman observations sample the molecular envelope of the northern molecular ridge; this envelope is defined by the C^{18}O distribution. Its size is about 0.5 × 0.3 pc (see Fig. 6). Using the expression stated by Wilson et al. (1995), which relates the observed line strength and width to N(CO), our C^{18}O $J = 1 \rightarrow 0$ data yield $\langle N_H \rangle \approx 0.8 \times 10^{23}$ cm^{-2} for the standard CO/H$_2$ ratio of 10^{-4}. Mauersberger et al. (1992) found $\langle N_H \rangle \approx (0.5\text{–}1.5) \times 10^{23}$ cm^{-2} based on C^{18}O $J = 2 \rightarrow 1$ observations; they pointed out that the C^{18}O line may be slightly saturated and N_H therefore underestimated by a factor of about 1.5. We adopt $\langle N_H \rangle = 1.5 \times 10^{23}$ cm^{-2}. The area of the cloud and its column density then yield $M \approx 200\ M_\odot$, allowing for 10% He. Taking the mean radius of the region to be 0.2 pc, we find $n_H \approx 1 \times 10^5$ cm^{-3}. The kinetic temperature of this envelope gas is $T_K \approx 20$ K (Mezger et al. 1992; Mauersberger et al. 1992). Line widths of OH (this paper) and C^{18}O (this paper; Mauersberger et al. 1992) are in the range $\Delta v \approx 1\text{–}2$ km s^{-1}; we adopt $\Delta v = 1.5$ km s^{-1}. Based on our Zeeman results, we adopt $|\boldsymbol{B}| = 100\ \mu$G for the *total* magnetic field strength. However, for all quantities involving the magnetic field strength one must remember that $|\boldsymbol{B}| = 100\ \mu$G is a lower limit, both because the intensity of the $v_{LSR} = 10.2$ km s^{-1} component is likely weaker than we have assumed and because the field may lie partially in the plane of the sky.

The last six rows of Table 2 give information calculated from the measured physical parameters. The first two are the ratio of the observed velocity dispersion ($\sigma = \Delta v/(8 \ln 2)^{1/2}$) to the isothermal sound speed ($c = (kT_K/\mu m_H)^{1/2}$) and to the Alfvén speed ($v_A = B/(4\pi\rho)^{1/2}$). The next row gives the ratio of the observed-to-critical mass-to-magnetic flux ratio ($(M/\Phi_B)_{obs/crit} = 4.8 \times 10^{-21} N_H/B$ cm^2 μG); this

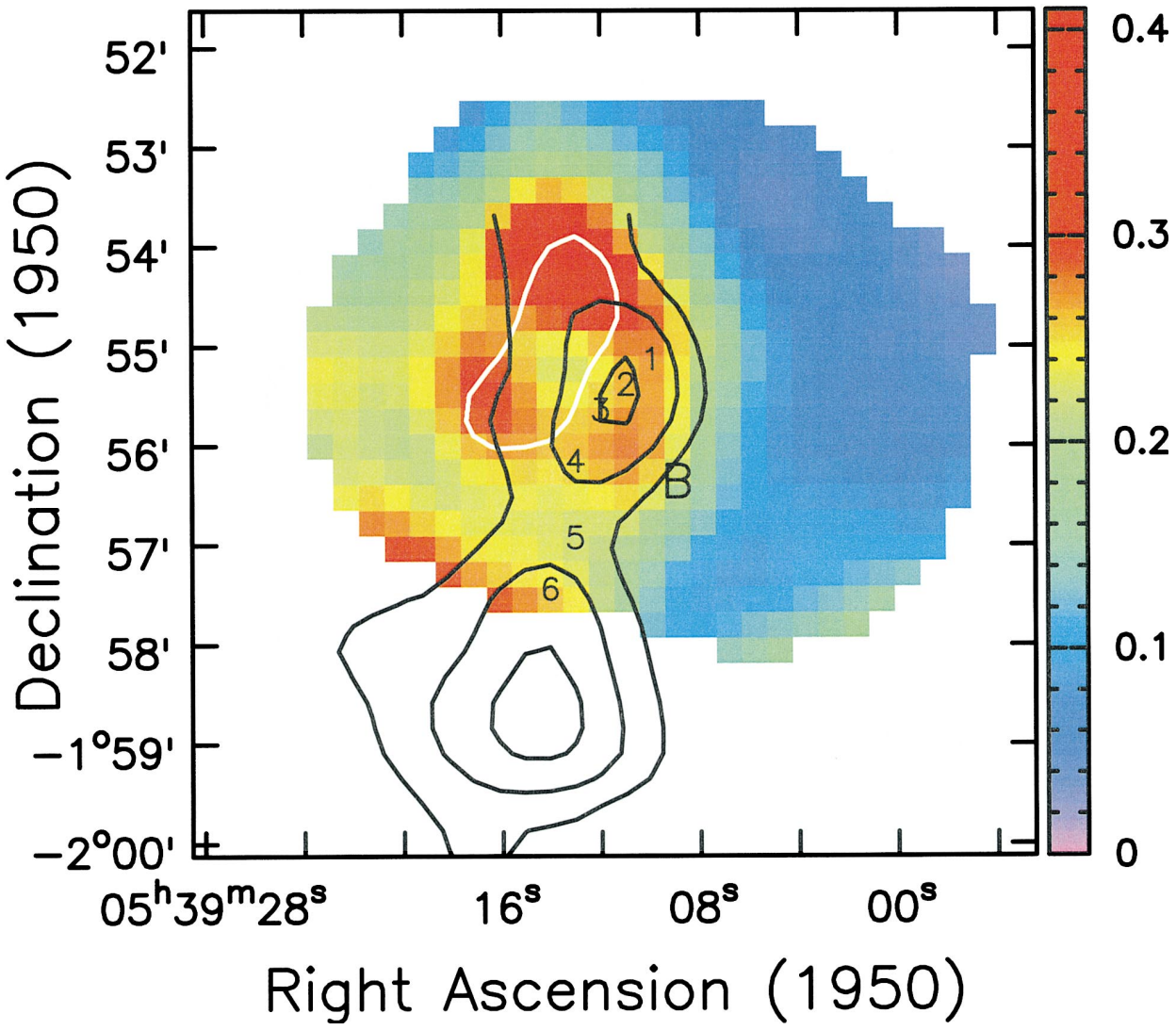

FIG. 6.—As in Fig. 5, except for $v_{LSR} = 10.2$ km s^{-1}. Also, the τ(OH) = 0.5 contour from Fig. 5 is reproduced here.

TABLE 2

MOLECULAR CLOUD RESULTS

Item	Value
Radius (pc)	0.2
Mass ($M_\odot$)	200
N_H (cm^{-2})	1.5×10^{23}
n_H (cm^{-3})	1×10^5
T_K (K)	20
ΔV (km s^{-1}).....	1.5
$\|\boldsymbol{B}\|$ (μG)	100
σ/c	2.4
σ/v_A	1.1
$(M/\Phi_B)_{obs/crit}$	7
$\boldsymbol{W}$ (ergs).....	1.0×10^{46}
$2\boldsymbol{T}/\boldsymbol{W}$.....	0.5
$\boldsymbol{M}/\boldsymbol{W}$	0.08

NOTE.—Values are as follows: σ is the line velocity dispersion, c is the speed of sound, v_A is the Alfvén velocity, M/Φ_B is the mass to magnetic flux ratio, $\boldsymbol{W}$ is the virial gravitational energy, $2\boldsymbol{T}$ is the virial thermal energy, and $\boldsymbol{M}$ is the virial magnetic energy

comes from the Mouschovias & Spitzer (1976) result $(M/\Phi_B)_{crit} = 1/(63G)^{1/2}$ and $\Phi_{B,obs} = B \times$ Area and $M_{obs} = 1.4N_H \times$ Area (allowing for 10% He). The final three rows give the virial energies (McKee et al. 1993) of the molecular ridge envelope. For the three virial energy terms we use gravitational energy $\boldsymbol{W} = 0.6GM^2/R$, kinetic energy $2\boldsymbol{T} = 3M\sigma^2$, and magnetic energy $\boldsymbol{M} = 0.33B^2R^3$. These expressions are for a uniform, spherical cloud and are therefore only approximately correct for more realistic cases; McKee et al. (1993) discussed various corrections to these expressions, but we use the simple expressions here.

The motions in the NGC 2024 molecular cloud are supersonic, a common result in molecular clouds. They are approximately equal to the Alfvén speed, however, which suggests that the supersonic motions that are observed may be due to magnetohydrodynamical waves (rather than hydrodynamical turbulence) in the molecular gas. The mass-to-magnetic flux ratio, M/Φ_B, is supercritical by a factor of ~ 7, which implies that the cloud is not supported by the static magnetic field we observe. This conclusion is reinforced by the values of the virial energy terms. The observed kinetic energy is nearly in equilibrium with the

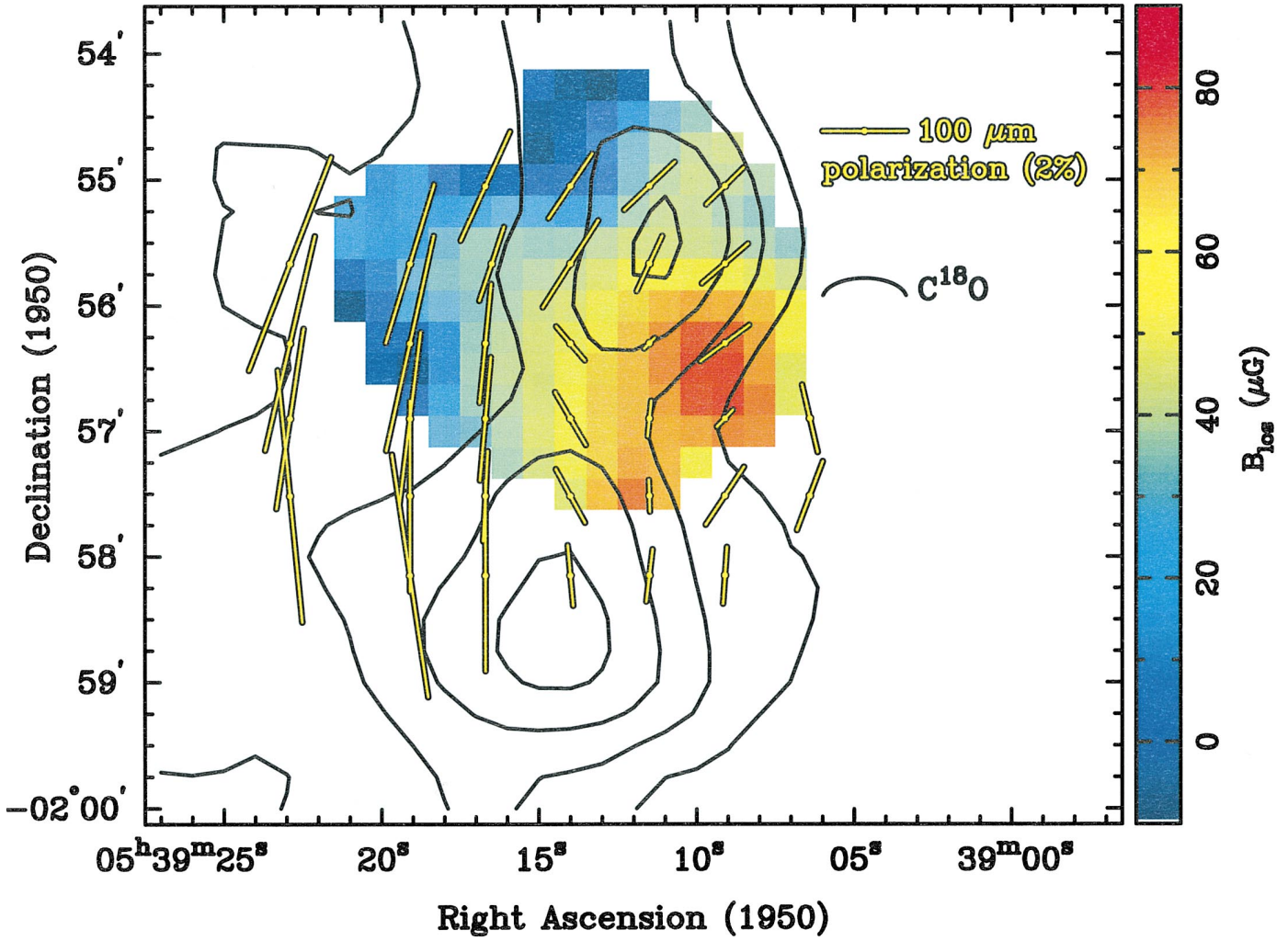

FIG. 7.—Maps of 100 μm dust continuum linear polarization (*yellow lines*), $C^{18}O$ emission (contours), and B_{los} (*color image*).

gravitational energy, whereas the magnetic energy is an order of magnitude lower. Although the kinetic energy is a factor of 2 lower than the gravitational energy, given the uncertainties in the measured physical parameters this difference may not be significant. Taken at face value, these results imply that nonthermal motions, not static magnetic fields, support the cloud against gravitational collapse. However, a factor of ~ 4 increase in $|\boldsymbol{B}|$ over our lower limit would bring the static magnetic field energy into equilibrium with the other energies and make the mass-to-magnetic flux ratio approximately critical rather than supercritical. We have no way of ruling out this larger magnetic field strength in a single cloud, where we can only measure B_{los} and not $|\boldsymbol{B}|$. Similar studies of a large number of clouds will eventually make it possible to apply statistical techniques to eliminate the limitation imposed by being able to observe the amplitude of only the line-of-sight component of $\boldsymbol{B}$ and to answer the question of the role that magnetic fields play in cloud physics and evolution.

6. CONCLUSIONS

We have produced maps of the OH and H I Zeeman effect toward the NGC 2024 molecular cloud. Our conclusions based on a comparison of these maps with information about the other physical parameters of the molecular cloud are the following:

1. The magnetic field that is mapped comes not from the entire velocity range of the absorption lines but from a subcomponent at $v_{LSR} \approx 10.2$ km s^{-1}. This subcomponent corresponds in velocity and in spatial morphology with the envelope of the northern dense molecular ridge in which the very dense dust clumps FIR 1–4 are embedded. Although this dense gas is probably behind most of the H II region, a small part of the H II continuum emission must come from behind the dense ridge. This requires that there be a clumpy structure in the gas.

2. Although the magnitude of B_{los} mapped in H I is lower than in OH, the morphologies of the field mapped in OH and H I agree very well. This may be a result of the H I Zeeman effect sampling slightly different (lower density) gas than does the OH.

3. B_{los} varies from 0 to the northeast of the northern molecular ridge to almost 100 μG to the southwest. A published map of linearly polarized dust emission shows a relative minimum in percentage polarization near the B_{los} maximum, which suggests that the variation in B_{los} may be due to the field being mainly in the plane of the sky to the northeast but having a significant line-of-sight component to the southwest.

4. Motions in the cloud are supersonic, but velocities are approximately equal to the Alfvén velocity, which is consistent with motions being dominated by magnetohydro-

dynamical waves rather than hydrodynamical turbulence.

5. The mass-to-magnetic flux ratio is supercritical by a factor of ~ 7, which suggests that the static magnetic field does not support the cloud against collapse. Simple virial estimates of the relative importance of gravitational, kinetic, and magnetic energies show that the ratio of kinetic/gravitational energy is about 0.5, while the magnetic/gravitational energy ratio is less than 0.1. At face value, these results imply that the cloud is supported mainly by nonthermal motions rather than by the static magnetic field. However, since we only measure directly the line-of-sight component of $\boldsymbol{B}$, this result is not conclusive.

This research has been supported in part by the National Science Foundation under grants NSF AST 94-19220 and NSF AST 94-19227.

REFERENCES

Anthony-Twarog, B. J. 1982, AJ, 87, 1213
Barnes, P. J., Crutcher, R. M., Bieging, J. H., Storey, J. W. V., & Willner, S. P. 1989, ApJ, 342, 883
Brogan, C. L., Troland, T. H., Roberts, D. A., & Crutcher, R. M. 1999, ApJ, 515, 304
Chandler, C. J., & Carlstrom, J. E. 1996, ApJ, 466, 338
Chandler, C. J., Moore, T. J. T., & Emerson, J. P. 1992, MNRAS, 256, 369
Crutcher, R. M., Henkel, C., Wilson, T. L., Johnston, K. J., & Bieging, J. H. 1986, ApJ, 307, 302
Crutcher, R. M., & Kazès, I. 1983, A&A, 125, L23
Hildebrand, R. H., Dotson, J. L., Dowell, C. D., Platt, S. R., Schleuning, D., Davidson, J. A., & Novak, G. 1995, in ASP Conf. Ser. 73, Airborne Astronomy Symposium on the Galactic Ecosystem: From Gas to Stars to Dust (San Francisco: ASP), 97
Mauersberger, R., Wilson, T. L., Mezger, P. G., Gaume, R., & Johnston, K. J. 1992, A&A, 256, 640
McKee, C. F., Zweibel, E. G., Goodman, A. A., & Heiles, C. 1993, in Protostars and Planets III, ed. E. H. Levy & J. I. Lunine (Tucson: Univ. Arizona Press), 327
Mezger, P. G., Chini, R., Kreysa, E., Wink, J. E., & Salter, C. J. 1988, A&A, 191, 44
Mezger, P. G., Sievers, A. W., Haslam, C. G. T., Kreysa, E., Lemke, R., Mauersberger, R., & Wilson, T. L. 1992, A&A, 256, 631
Moore, T. J. T., Chandler, C. J., Gear, W. K., & Mountain, C. M. 1989, MNRAS, 237, 1P
Mouschovias, T. Ch. & Spitzer, L., Jr. 1976, ApJ, 210, 326
Roberts, D. A., Crutcher, R. M., & Troland, T. H. 1995, ApJ, 442, 208
Roberts, D. A., Crutcher, R. M., Troland, T. H., & Goss, W. M. 1993, ApJ, 412, 675
Snell, R. L., Mundy, L. G., Goldsmith, P. F., Evans, N. J., II, & Erickson, N. R. 1984, ApJ, 276, 625
Schulz, A., Gusten, R., Zylka, R., & Serabyn, E. 1991, A&A, 246, 570
Schwarz, U. J., Troland, T. H., Albinson, J. S., Bregman, J. D., Goss, W. M., & Heiles, C. 1986, ApJ, 301, 320
van der Werf, P. P., Goss, W. M., Heiles, C., Crutcher, R. M., & Troland, T. H. 1993, ApJ, 411, 247
Wiesemeyer, H., Gusten, R., Wink, J. E., & Yorke, H. W. 1997, A&A, 320, 287
Wilson, T. L., Mehringer, D. M., & Dickel, H. R. 1995, A&A, 303, 840